Quantification of DNA Structure from NMR Data: Conformation of d-ACATCGATGT

K. V. R. Chary, Sandeep Modi, R. V. Hosur, and Girjesh Govil*
Chemical Physics Group, Tata Institute of Fundamental Research, Homi Bhabha Road, Colaba, Bombay 400005, India
Chang-qing Chen‡ and H. Todd Miles*
Laboratory of Molecular Biology, National Institute of Diabetes and Digestive and Kidney Diseases, National Institutes of Health, Bethesda, Maryland 20892
Received November 8, 1988; Revised Manuscript Received February 22, 1989

ABSTRACT: Resonance assignments of nonexchangeable base and sugar protons have been obtained in double-helical d-ACATCGATGT by using two-dimensional correlated spectroscopy (COSY) and nuclear Overhauser enhancement spectroscopy (NOESY). The exchangeable imino protons have been assigned on the basis of their chemical shifts. The characteristic phase-sensitive multiplet patterns of the intrasugar cross-peaks in the ω_1-scaled COSY spectrum have been used to estimate several scalar coupling constants (J). The information on the J values combined with the intranucleotide COSY cross-peak intensities has been used to identify sugar puckers of individual nucleotide units. In most cases, the deoxyribofuranose rings are found to adopt a conformation close to O4′-endo. Spin diffusion has been monitored from the buildup of the normalized volumes of NOE cross-peaks in NOESY spectra as a function of mixing time. A set of 52 intranucleotide and internucleotide proton–proton distances have been estimated by using low mixing time NOESY spectra (τ_m = 40 and 80 ms). The estimated intrasugar proton–proton distances rule out possibilities of existence of a fast equilibrium between C2′-endo and C3′-endo conformations. Intranucleotide proton–proton distances combined with the knowledge of sugar puckers have been used to fix the glycosidic bond torsion angle (χ). For this purpose, simulated distance contours depicting the dependence of intranucleotide proton–proton distances on pseudorotational phase angle (P) and glycosidic bond torsion angle (χ) have been used. Further, the proton homonuclear (J, δ) spectrum has been used to monitor the ^{31}P–^1H heteronuclear couplings, which are preserved in the ω_2 projection. Such J values provide information on the backbone torsion angle (ϵ) (C3′–O3′–P–O5′). It is observed that the molecule adopts an overall conformation close to the right-handed B-DNA, although there are subtle variations in the details of the sequence-dependent structure.

The specific interaction between proteins and nucleic acids constitutes an important problem in molecular biology. Our own interests have been in DNA fragments recognized and cleaved by restriction enzymes. In such an intermolecular interaction, structures of the individual molecules may play a dominant role. In view of this, we have been working toward obtaining accurate solution structures of protein binding segments of DNA using two-dimensional NMR techniques. New strategies have been developed (Chary et al., 1988; Chary & Modi, 1988; Hosur et al., 1988a,b) for precise and detailed structural information from the experimental 2D NMR spectra. Structures have been obtained for the following double-helical DNA segments: (I) d-GGATCCGGATCC (Hosur et al., 1985a; Ravikumar et al., 1985); (II) d-GAATTCGAATTC (Chary et al., 1987; Hosur et al., 1986a); (III) d-CTCGAGCTCGAG (Sheth et al., 1987a); (IV) d-GAATTCCCGAATTC (Hosur et al., 1986b); (V) d-CGCGCGCGCGCG (Sheth et al., 1987b); and (VI) d-GGTACGCGTACC (Chary et al., 1988).

The general strategy adopted for obtaining the detailed structural information is as follows: (i) Use of quantitative information about the intrasugar proton–proton vicinal coupling constants and proton–proton distances for fixing the pseudorotation phase angle (P). (ii) Combined use of the knowledge about the angle P and the intranucleotide interproton distances [more specifically the distance between base proton (H6/H8) and the sugar protons (H1′, H2′, H2″, H3′, and H4′)] for elucidation of precise values of glycosidic bond torsion angles (χ). (iii) Estimation of ^{31}P–H3′ coupling constants from the projection of homonuclear two-dimensional (J-δ) proton spectra for obtaining the backbone torsion angle (ϵ). (iv) Combined use of the knowledge about individual P's, χ's, ϵ's, and four different sequential internucleotide (intrastrand) distances [involving the base proton (H6/H8) of ith nucleotide unit and the base and sugar protons (H6/H8, H1′, H2′, and H2″) of the $(i-1)$th nucleotide unit] for obtaining information about other backbone torsion angles.

In this paper, we report sequence-specific ^1H resonance assignments, estimation of sugar ring proton–proton coupling constants, and intramolecular interproton distances in d-ACATCGATGT (VII) using COSY, ω_1-scaled COSY, and ω_1-scaled NOESY. This molecule has specific cleavage sites for the restriction endonucleases *Taq*I and *Cla*I (Figure 1). *Taq*I recognizes the TCGA fragment and cleaves between T and C, whereas *Cla*I recognizes the sequence ATCGAT and also cleaves between T and C.

Materials and Methods

(*a*) *Synthesis.* d-ACATCGATGT was prepared by a manual method on controlled pore glass (CPG) using cyanoethyl phosphoramidite chemistry (McBride & Caruthers, 1983; Sinha et al., 1984; Atkinson & Smith, 1984). We

* Authors to whom correspondence should be addressed.
‡ Permanent address: Shanghai Centre of Biotechnology, Chinese Academy of Sciences, Shanghai, China.

0006-2960/89/0428-5240$01.50/0

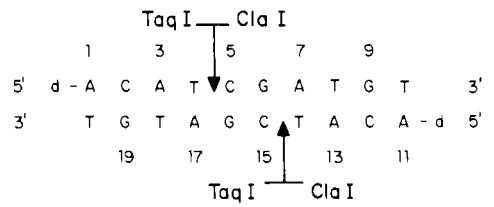

FIGURE 1: Cleavage sites for restriction endonuclease *Taq*I and *Cla*I. The corresponding recognition segments are TCGA and ATCGAT, respectively.

employed unidirectional flow of reagents under argon pressure through a column filled with CPG loaded with 25 μmol of 3′-bound T. After detritylation, cleavage from column, and deprotection, the oligomer was purified on DEAE-cellulose with a 0–0.8 M gradient of ammonium bicarbonate in 7 M urea [cf. Staehelin et al. (1959) and Tomlinson and Tener (1963)]. A central cut of the main peak was diluted and placed on DEAE-cellulose for removal of urea and then eluted with 0.8 M NaCl. After dialysis, the purified product consisted of 24 mg or 630 AU. The material was homogeneous on 20% acrylamide gel containing 8 M urea.

(*b*) *Sample Preparation.* For the ^{1}H NMR experiments 10 mg of d-ACATCGATGT was dissolved in 400 μL of 50 mM sodium phosphate buffer (pH 7.3) and 1 mM ethylenediaminetetraacetic acid (EDTA). The solution was repeatedly lyophilized from ^2H_2O solution. Finally the sample was made up to 0.4 mL with 99.95% ^2H_2O. For the NMR experiments in H_2O the same sample was dissolved in water and lyophilized repeatedly. Finally the sample was made up to 0.4 mL with a mixture consisting of 80% H_2O and 20% ^2H_2O.

(*c*) *Nuclear Magnetic Resonance Spectroscopy.* ^{1}H spectra were recorded on a Bruker AM-500 FT-NMR spectrometer equipped with an ASPECT 3000 computer. The spectrum in H_2O was recorded with a 1–3–3–1 selective excitation pulse sequence for water suppression (Hore, 1983). COSY data were recorded by using a (RD–90–t_1–Δ–90–Δ–t_2) pulse sequence, where Δ is the fixed delay (5 ms) used for the enhancement of cross-peaks (Bax & Freeman, 1981; Anil Kumar et al., 1984; Hosur et al., 1985; Wynants & Van Binst, 1984). The time domain data set consisted of 2048 and 512 data points along t_2 and t_1 domains, respectively. The number of transients collected for each t_1 value was 64. The data set was zero filled to 1024 along the t_1 axis and was multiplied by unshifted sine-square bell and unshifted sine bell window functions along the t_2 and t_1 axes, respectively, before two-dimensional Fourier transformation. The digital resolution along both the axes was 7.5 Hz/point.

Two-dimensional homonuclear (J, δ) spectrum in ^2H_2O at 35 °C was recorded with the conventional pulse sequence 90–t_1/2–180–t_1/2–FID. The time domain data consisted of 4096 t_2 and 32 t_1 points. Such data were zero filled to 8192 and 128 along the t_2 and t_1 axes, respectively, and multiplied by phase-shifted (π/32) sine bell window functions along both the axes prior to the two-dimensional Fourier transformation. The spectra were processed in the absolute value mode.

All other two-dimensional NMR spectra were recorded in the phase-sensitive mode by using the time proportional phase incrementation method (Redfield & Kunz, 1975; Marion & Wüthrich, 1983). A phase-sensitive ω_1-scaled COSY (Hosur et al., 1985c, 1988a,b) spectrum was recorded with the shift scaling factor α of 0.5 and J scaling factor γ of 1.5. The time domain data set consisted of 2048 and 450 data points along t_2 and t_1 domains, respectively. The number of transients collected for each t_1 value was 64. The data set was zero filled to 4096 and 2048 along the t_2 and t_1 axes, respectively, and was multiplied by sine bell (shifted by π/16) along both axes before the 2D Fourier transformation. The spectral offset was placed at the center of the spectrum. The spectral width was optimized to derive maximum possible digital resolution by allowing a part of the base proton region to fold up to 6.4 ppm. The resultant digital resolution along both the axes was 1.5 Hz/point.

Absorption mode ω_1-scaled NOESY (Hosur et al., 1988b) spectra of the decamer in ^2H_2O solution were recorded under identical conditions using mixing times of 20, 40, 60, 80, 120, and 150 ms. In all experiments the mixing time was randomly varied by 3% to suppress the contributions from zero and residual double-quantum coherences evolving during the mixing time. In the NOESY spectrum all the components of individual cross-peaks are in-phase absorptive, and the scaling factors α and γ (0.5 and 0.6, respectively) help to enhance both the sensitivity and resolution in the spectra. In each of these experiments the spectral offset was placed at the center of the spectrum, and 1024 and 256 data points were collected along t_2 and t_1 dimensions. The data sets were zero filled to 2048 and 1024 data points along the t_2 and t_1 axes and multiplied by cosine bell window functions before the two-dimensional Fourier transformation. The resultant digital resolution along both the axes was 3.7 Hz/point.

The melting temperature of ACATCGATGT has been determined to be 45 °C in 0.1 M Na^+ from UV experiments. The temperature at which all the NMR measurements were carried out (25 °C) is therefore in the range in which the decamer is in an ordered form.

Results and Discussion

(*a*) *Resonance Assignment.* ^{1}H NMR spectra (500 MHz) of nonexchangeable and exchangeable imino protons (inset) of d-ACATCGATGT, recorded from ^2H_2O and 80% H_2O plus 20% ^2H_2O solutions, respectively, are shown in Figure 2. Sequence-specific assignment of nonexchangeable protons has been carried out following well-established procedures (Chary et al., 1987; Chazin et al., 1986; Clore & Gronenborn, 1985a; Feigon et al., 1982, 1983a,b; Frechet et al., 1983; Hare et al., 1983; Hosur et al., 1985a; Reid et al., 1983; Scheek et al., 1983, 1984). The efficient spin diffusion occurring among the sugar protons of individual nucleotide units resulted in the observation of H3′–H5′,H5″ NOESY cross-peaks. This has been utilized for assigning H5′ and H5″ sugar protons of A1, A3, G6, A7, and G9. All the assignments are listed in terms of the chemical shifts of various protons in Table I. The imino proton resonances of the base pairs are easily assigned on the basis of their chemical shifts. Imino protons of AT base pairs resonate downfield compared to those of GC pairs. The peak at ~12.4 ppm has twice the intensity of those at ~13.5 ppm, indicating that it accounts for twice as many imino protons as the individual peaks around 13.5 ppm. Taking into consideration the symmetry in the sequence of the molecule, the imino protons can be easily assigned as indicated in Figure 2. For example, AT base pairs at positions 3 and 8 are equivalent and so is the case with positions 4 and 7. All the GC pairs show accidental equivalence and their imino protons resonate at ~12.4 ppm. The terminal imino protons are not observed due to rapid exchange with water.

(*b*) *3D Structure of the Oligonucleotide.* Observation of four resonance lines in the imino proton region (11–14 ppm) of the one-dimensional NMR spectrum (Figure 2) confirms the results from UV and IR measurements (F. B. Howard, C. Chen, J. Frazier, and H. T. Miles, unpublished experiments) that the molecule is in double-helical form under the present experimental conditions. Qualitative analysis of the relative

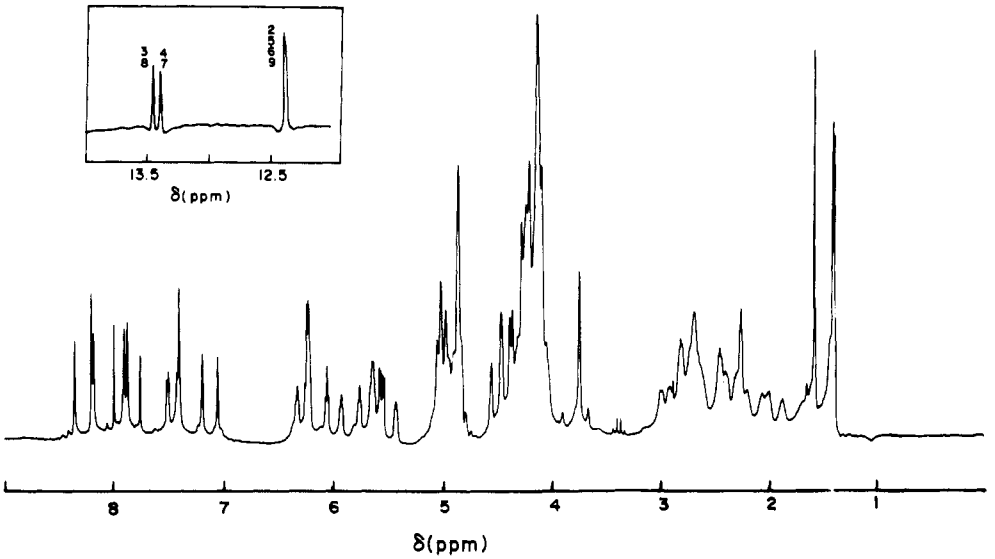

FIGURE 2: One-dimensional 500-MHz ^1H NMR spectra of nonexchangeable and exchangeable imino protons (inset) in d-ACATCGATGT recorded by using 5 mM solution in ^2H_2O and 80% H_2O plus 20% ^2H_2O (pH 7.3) solutions, respectively, at 25 °C. The spectrum in the inset was obtained with 1-3-3-1 selective excitation pulse sequence. Assignments of imino proton resonances are indicated by numbers corresponding to the sequential positions of the base pairs.

Table I: Chemical Shifts of Nonexchangeable Protons in d-ACATCGATGT Expressed with Respect to Sodium 3-(Trimethylsilyl)[2,2,3,3-^2H]propionate (TSP) at 25 °C

nucleotide unit	H1′	H2′	H2″	H3′	H4′	H5′	H5″	H6/H8	H5/CH_3/H2
A1	6.19	2.62	2.78	4.84	4.23	3.70	3.70	8.18	–
C2	5.39	2.17	2.41	4.85	4.16	–	–	7.48	5.50
A3	6.29	2.72	2.95	5.02	4.44	4.10	4.18	8.33	7.97
T4	5.89	2.03	2.43	4.85	4.18	–	–	7.16	1.37
C5	5.60	1.97	2.37	4.83	4.09	–	–	7.40	5.54
G6	5.61	2.69	2.79	5.00	4.32	4.00	4.10	7.87	–
A7	6.18	2.59	2.89	4.99	4.43	4.09	4.21	8.15	7.97
T8	5.72	1.85	2.28	4.83	4.09	–	–	7.07	1.35
G9	6.02	2.65	2.65	4.95	4.35	4.10	4.10	7.84	–
T10	6.21	2.23	2.23	4.52	4.07	–	–	7.36	1.52

NOESY cross-peak intensities (Figure 3) reveals that the structure belongs to the right-handed B-DNA family (Chary et al., 1987, 1988; Hosur et al., 1985a). Observation of internucleotide NOEs (H8 of A3 to CH_3 of T4; H8 of A7 to CH_3 of T8; H6 of T4 to H5 of C5; H8 of G9 to CH_3 of T10) further establishes the right-handed sense of the helix. A more precise quantitative description of the 3D structure of the oligomer has been obtained by measurement of proton–proton scalar coupling constants (J) and proton–proton distances (r) from the phase-sensitive ω_1-scaled 2D-COSY and 2D-NOESY spectra, respectively.

(*c*) *Estimation of Scalar Coupling Constants* (J). As discussed earlier (Chary et al., 1988; Hosur et al., 1986a) there are five three-bond vicinal coupling constants (H1′–H2′, H1′–H2″, H2′–H3′, H2″–H3′, and H3′–H4′) that show strong dependence on the conformation of the deoxyribose ring. The conformational dependence of such J values has been established [see, for example, Chary et al. (1987, 1988), Hosur et al. (1986a,b), and Rinkel and Altona (1987)]. Theoretical values for some selected conformations are listed in Table II along with the experimental results for the convenience of the discussion in the following paragraphs.

Experimental quantification of the J values for the deoxyribose rings even in a medium-size DNA fragment is difficult due to problems of resolution. Recently it has been shown that simultaneous scaling of chemical shifts and coupling constants in phase-sensitive correlated spectroscopy improves the resolution significantly (Chary et al., 1988; Hosur et al., 1985c, 1988a,b; Chazin et al., 1986). This technique has been used to resolve individual components of the H1′–H2″ and H1′–H2′ phase-sensitive cross-peaks (Figure 4). As discussed earlier (Chary et al., 1988; Hosur et al., 1988a,b), the ω_2 axis in H1′–H2″ cross-peaks contains information about J(H1′–H2″),

Table II: Experimentally Observed and Theoretically Expected Intrasugar Interproton Coupling Constants (J) in d-ACATCGATGT at 25 °C

nucleotide unit	H1′–H2′	H1′–H2″	H2′–H3′	H2″–H3′	H3′–H4′	H2′–H2″
			Experimental Values			
A1	8.4	7.0	8.9	w, ≤3	m	−14.5
C2	8.3	6.6	8.2	a, ≤3	m	−14.2
A3	7.9	6.9	8.5	a, ≤3	m	−15.2
T4	8.2	7.2	9.6	a, ≤3	m	−14.3
C5	7.7	7.3	7.8	a, ≤3	m	−14.7
G6	8.9	6.9	8.8	a, ≤3	m	−14.0
A7	7.8	7.0	8.5	a, ≤3	m	−14.3
T8	7.3	7.1	9.1	a, ≤3	m	−14.4
G9	o	o	o	o	s	o
T10	o	o	o	o	s	o
			Theoretically Estimated Values			
C3′-endo	0.0	7.2	6.0	9.5	9.0	−14.0
O4′-endo	7.0	8.0	9.5	3.0	7.0	−14.0
C1′-exo	9.0	6.0	8.5	0.0	3.0	−14.0
C2′-endo	9.0	6.0	6.0	0.0	0.0	−14.0

[a] Estimates of J(3′–4′) are reflected in the intensities of the respective cross-peaks in the low-resolution COSY spectrum: *a* = peak absent (very small J), m = medium peak (moderately large J), s = strong peak (large J), o = peaks overlap, w = weak peak (small J). The accuracy of experimental coupling constants measured is ±0.3 Hz.

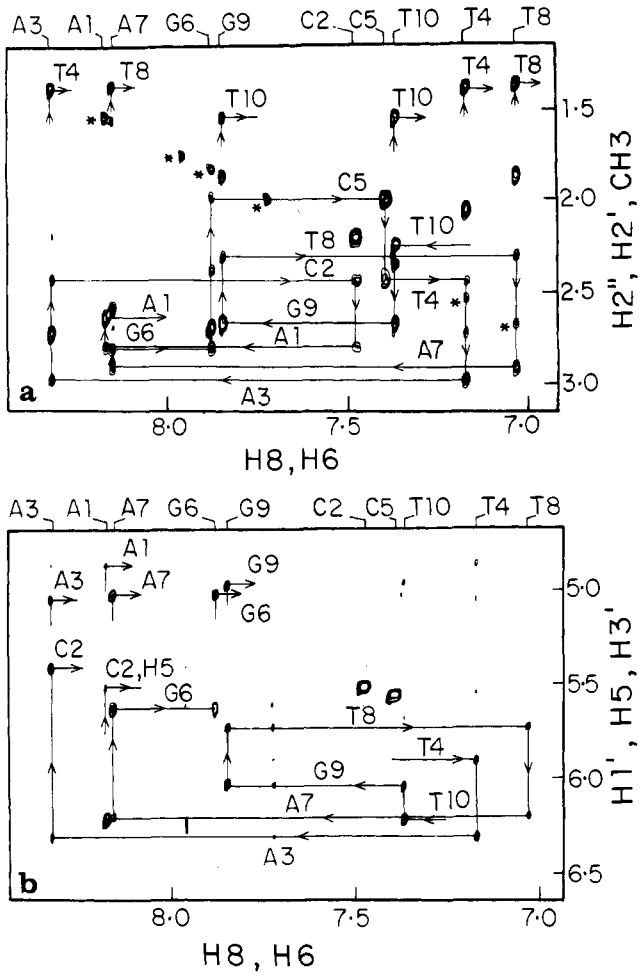

FIGURE 3: Selected regions of pure absorption ω_1-scaled NOESY spectrum recorded with a mixing time of 80 ms. (a) Sequential connectivities between H6/H8 protons and H2′/H2″ sugar protons (d3 pathways) and between base H6/H8 protons and base CH_3 protons (d1 pathways). (b) Sequential connectivities using H6/H8 protons and H1′ sugar protons (d2 pathways). This section also contains intranucleotide NOESY connectivities between base H6/H8 protons and sugar H3′ protons. The peaks marked by asterisks are artifacts due to imperfections in quadrature detection. These can be detected easily as they lie on a diagonal.

J(H2′–H2″), and J(H2″–H3′), while the ω_1 axis has information about J(H1′–H2′) and J(H1′–H2″). Consequently, individual cross-peaks are expected to show 8 × 4 multiplet patterns. For most nucleotides one is able to resolve 16 components, the only exceptions being G9 and T10. Such a resolution helps in quantifying J(H1′–H2′), J(H1′–H2″), and J(H2′–H2″) within an error of ±0.3 Hz. Evidently, J(H2″–H3′) is buried in the line width and hence can be considered to be less than 3 Hz. The values of estimated coupling constants are listed in Table II. In the case of G9 and T10, identical shift values of H2′ and H2″ proton resonances render it impossible to resolve them. Of the remaining two J values, namely, J(H2′–H3′) and J(H3′–H4′), the former can be obtained from the multiplicity pattern of the H1′–H2′ cross-peak. Even though these cross-peaks are not resolved into their individual components because of their complex (16 × 8) multiplicity patterns, the separation between the farthest components of H1′–H2′ cross-peaks [which is equal to J(H2′–H1′) + J(H2′–H2″) + J(H2′–H3′)] could be measured in the case of the first eight (A1–T8) nucleotide units. Thus, with the earlier knowledge of J(H1′–H2′) and J(H2′–H2″) the value of J(H2′–H3′) can be estimated. These values are also listed in Table II. Once again, because of the near equivalence of H2′ and H2″ proton resonances, information about the J(H2′–H3′) coupling constant could not be obtained in the case of G9 and T10.

The remaining coupling constant J(H3′–H4′) could not be estimated due to the following reasons: (i) complex multiplicity (8 × 16) of the H3′–H4′ cross-peak; (ii) small dispersions in both the H3′ and H4′ chemical shifts; and (iii) dispersive line shapes of diagonal peaks in ω_1-scaled phase-sensitive COSY spectrum. The tails of dispersive peaks spread over the region of H3′–H4′ cross-peaks and mask them completely. However, comparison of relative intensities of the COSY cross-peaks in the low-resolution COSY spectrum (Figure 5a,b) has been helpful in qualitative assessment of the magnitudes of J(H3′–H4′) coupling constants in all 10 nucleotides of the decamer. Such information is also presented in Table II.

(*d*) *Estimation of Intramolecular Proton–Proton Distances* (r). Intramolecular proton–proton distances (r) have been obtained from pure absorption ω_1-scaled NOESY spectra following the procedure described earlier (Chary et al., 1987; Hosur et al., 1988b). As a prelude to such estimation, we have monitored the buildup of some of the NOE volumes (Kumar et al., 1981; Chary et al., 1988; Wagner & Wüthrich, 1979) for intra- and internucleotide cross-peaks in the decamer to estimate the rates of spin diffusion. The buildup curves are shown for a few cross-peaks in Figure 6. The different rates of the NOE buildup curves indicate differences in the cross-relaxation rates for different peaks. From the viewpoint of spin diffusion it is desirable to use the smallest feasible mixing time for the distance estimation. However, at very low mixing time such as 20 ms, there may be some overestimation of volumes due to finite contributions from zero quantum coherences in spite of 3% random variation of the mixing time. Therefore, we have used NOESY spectra with mixing time between 40 and 80 ms for the estimation of interproton distances. The values of distances obtained, corresponding to 40 and 80 ms for each proton pair, are fairly close in almost all cases. The distances estimated by using 40-ms mixing time spectra are given in Table III. The blanks in this table are either due to extensive overlaps (o) of the corresponding NOESY cross-peaks that interfere with the precise measurements of volumes or due to the absence of the corresponding peaks (a).

The interproton distances have been estimated by using three different sets of reference distances, namely, thymine H6–CH_3 (3.00 Å), cytosine H6–H5 (2.45 Å), and sugar ring H2′–H2″ (1.85 Å) distances. The distances estimated by using the H2′–H2″ scale were found to be considerably shorter compared to the distances estimated by using the other two standards. We attribute the underestimation with the H2′–H2″ scale to significant contributions coming from J coupling correlations ($J \sim 14$ Hz) to the NOESY cross-peaks corresponding to these two protons. The choice between the other two standards is somewhat less obvious. While the J(H5–H6) of 8 Hz may provide some J coupling correlation to the NOESY cross-peaks, the use of thymine H6–CH_3 depends on a standard distance that may be modulated by rotation of the C–CH_3 bond. Distances using both C(H5–H6) and T(H6–CH_3) standards are given in Table III. The distances using the first standard are usually 0.3–0.4 Å lower.

(*e*) *Conformation of the Deoxyribofuranose Rings.* Conformations of the deoxyribofuranose rings in individual nucleotide units of d-ACATCGATGT have been determined from the independent knowledge of the intrasugar proton–proton vicinal coupling constants and proton–proton distances. Table II shows the experimentally measured values of vicinal

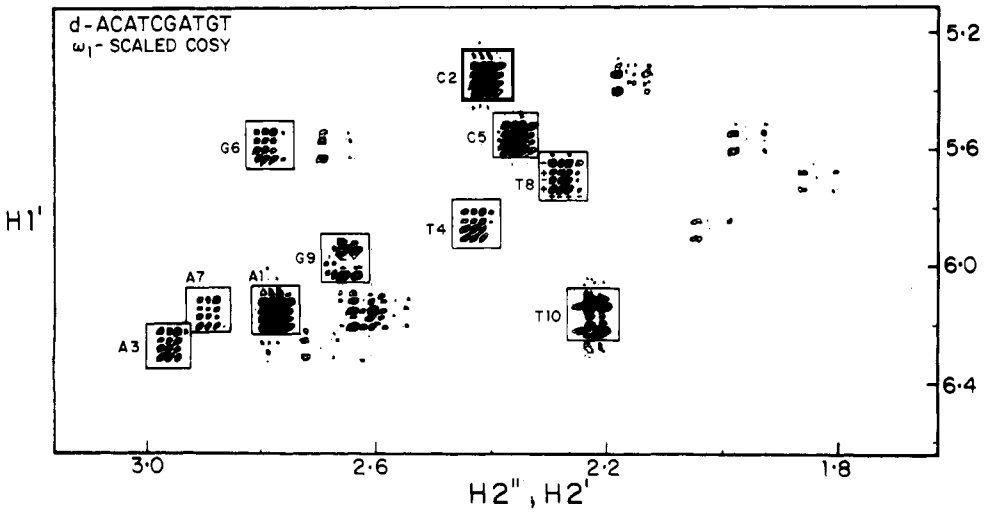

FIGURE 4: Selected region of 500-MHz ω_1-scaled phase-sensitive COSY spectrum of d-ACATCGATGT recorded in ^2H_2O at 25 °C, covering the expected H1′–H2′ and H1′–H2″ cross-peaks. Boxed portions in this figure show the characteristic phase-sensitive multiplet patterns of H1′–H2″ cross-peaks belonging to different nucleotide units. These portions help in the estimation of J(H1′–H2′), J(H1′–H2″), and J(H2′–H2″) values. Unboxed portions depict the H1′–H2′ cross-peak multiplet patterns. Though these could not be resolved into individual components, they could be used to estimate the value of J(H2′–H1′) + J(H2′–H2″) + J(H2′–H3′). The digital resolution along the ω_1 and ω_2 axes is 1.5 Hz/point.

coupling constants in the sugar ring of d-ACATCGATGT along with expected J values for some standard sugar geometries. Nonzero values of J(H1′–H2′) and J(H3′–H4′) rule out the possibility of traditional C3′-endo and C2′-endo sugar puckers in all 10 nucleotides. Comparison of the theoretical and experimental coupling constants reveals that conformations of sugars A1 and T8 lie between O4′-endo (P = 90°) and C1′-exo (P = 126°). In the case of G9 and T10 the situation is complicated by the near equivalence of H2′ and H2″ protons. However, the general behavior of the intensity patterns in low-resolution COSY (magnitude mode) (Figure 5a,b) leads us to believe that the conformation in the two cases is in the range P = 70–90° (Chary et al., 1987, 1988; Hosur et al., 1986a).

We have also used the alternative approach based on interpretation of intrasugar ring proton–proton distances (Chary & Modi, 1988) to obtain details of the sugar geometries. Such distances have been calculated theoretically for different P values by making use of bond distances, bond angles, and torsion angles as input parameters. The intrasugar ring torsion angles used in these calculations have been chosen from the conformation wheel in the pseudorotational representation for D-deoxyribose (Altona & Sundaralingam, 1972; Saran et al., 1973). We have checked the reliability of our simulations by accurate model building. Figure 7 shows the plots of the intrasugar ring interproton distances as a function of P. Similar plots have been reported by Wüthrich (1986). However, we observe several differences in the magnitudes of distances reported by him and those in Figure 7. For example, in the present calculations, the H1′–H4′ distance is found to vary between 2.8 and 4.1 Å. From these plots it is evident that H1′–H3′ and H2′–H4′ intrasugar proton–proton distances are invariably greater than 3.7 Å for all values of P, and one does not expect NOESY cross-peaks of appreciable intensities at low mixing times. The H1′–H2″ and H2′–H3′ interproton distances are the shortest and vary in a narrow domain of 0.2 Å. These proton pairs therefore give rise to strong NOESY peaks that are insensitive to the angle P. Similarly, H1′–H2′, H2″–H3′, and H3′–H4′ distances are also insensitive to the value of P. However, the H1′–H4′ and H2″–H4′ distances show strong dependence on the sugar pucker. These distances vary between 2.8 and 4.2 Å and can be used for establishing the sugar ring conformation and in discussions about any possible coexistence of more than one state in fast equilibrium on the NMR time scale. Qualitatively, for a C3′-endo conformation (P = 18°) one expects a strong H2″–H4′ NOESY cross-peak and a weak H1′–H4′ peak. In the case of C2′-endo (P = 162°) both H1′–H4′ and H2″–H4′ cross-peaks will be weak and H2″–H4′ may even be absent. Lastly, in the case of a sugar pucker centered around O4′-endo (P = 90°), the H1′–H4′ peak will be quite strong while H2″–H4′ may be absent. An important point that emerges from such simulations is the fact that there is a narrow range of P angles (50–120°) where the H1′–H4′ peaks will be significantly stronger than the H1′–H2′ peaks.

Figure 8 shows a section of the pure absorption NOESY spectrum recorded with a mixing time of 80 ms. The figure covers the range of frequencies where the cross-peaks between H1′ and other sugar protons are expected to appear. From this figure and the measured distances reported in Table IIIA, we note the following:

(i) The patterns show as expected that the H1′–H2″ cross-peaks are stronger than other cross-peaks. This distance is relatively insensitive to the sugar pucker, and the distances estimated from model simulations lie in a narrow domain of 2.1 and 2.4 Å. The measured values with the cytosine (H5–H6) scale are therefore in better agreement than those obtained by using the thymine (H6–CH_3) distance as a yardstick. The fact that both H1′–H2′ and H1′–H2″ distances lie in the domains expected from Figure 7 provides confidence that problems associated with spin diffusion and the use of H5–H6 distance as a calibration scale do not perturb measured distances to an appreciable extent.

(ii) The H1′–H3′ peaks are absent in all cases. Figure 7 shows that this distance lies between 3.5 and 4.2 Å. Thus, under the experimental conditions used for Figure 8, cross-peaks corresponding to distances larger than ca. 3.8 Å are likely to be absent. Under the same conditions, thymine (H6–CH_3) peaks ($r \sim 3$ Å) are observed with reasonably good signal to noise ratio. The fact that H2″–H4′ cross-peaks are not observed indicates that this distance is appreciably larger than 3 Å. This observation rules out possibilities of sugar conformations in the N domain for all the nucleotide units in d-ACATCGATGT.

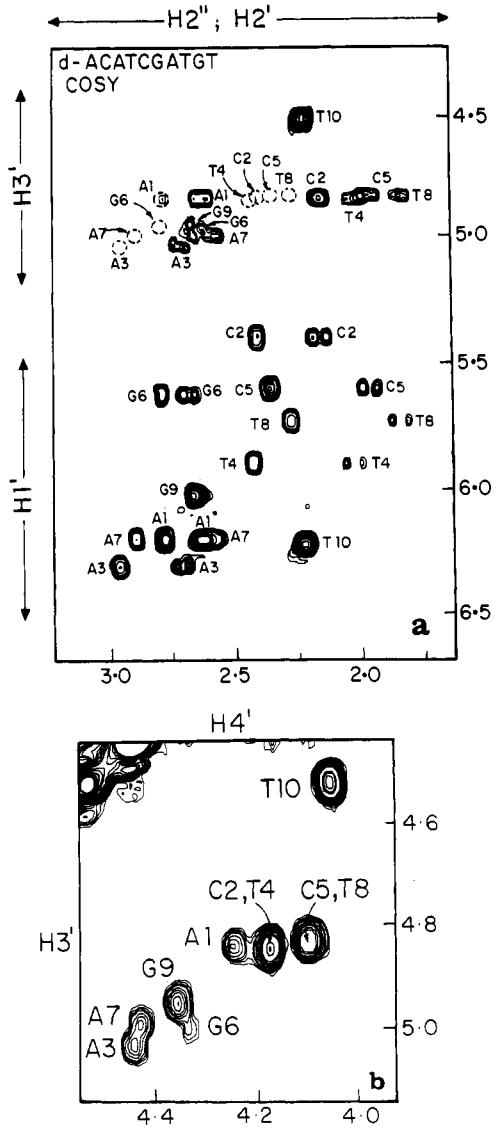

FIGURE 5: Expansion of selected portion of 500-MHz proton COSY spectrum of d-ACATCGATGT in ^2H_2O at 25 °C. (a) All the expected J coupling correlations for H1′–H2′, H1′–H2″, and H2′–H3′. The expected regions of the absent or very weak H2″–H3′ cross-peaks are indicated with dashed circles. (b) All the expected J coupling correlations for H3′–H4′.

(iii) In most cases, H1′–H4′ cross-peaks are stronger than H1′–H2′ peaks. Consequently, the measured H1′–H4′ distances are usually shorter than the H1′–H2′ distance. These observations rule out conformations with $P > 120°$, including the C2′-endo conformation ($P = 162°$) for which the H1′–H4′ distance is 3.4 Å and the H1′–H2′ distance is 3.0 Å.

(iv) The measured values of r(H1′–H4′) using C(H5–H6) as a yardstick lie in the range 2.6–3.1 Å. The three cases where this distance could not be estimated due to peak overlaps are C2, C5, and A7. The above values of measured distances confirm the conclusions reached from the J data that the sugar conformations in d-ACATCGATGT lie in the domain of O4′-endo ($P = 90°$) and C1′-exo ($P = 126°$). In fact, the condition r(H1′–H4′) < r(H1′–H2′) is satisfied only in a very narrow domain of P values (see Figure 7).

(v) In studies on solution conformations of randomly coiled oligonucleotides, the NMR data have often been interpreted in terms of a dynamic equilibrium between two states, C2′-endo and C3′-endo (Govil & Hosur, 1982). In view of arguments presented in (ii) and (iii) above, such a situation can be ruled out in the present case. For example, the theoretically estimated distance H1′–H4′ is greater than 3.4 Å for both C2′-endo and C3′-endo geometries. No combination of these two conformers can lead to the measured distances in the range 2.6–3.1 Å. In fact, the condition r(H1′–H4′) < r(H1′–H2′) established from NOESY cross-peak patterns shows that the molecular dynamics of sugar rings in d-ACATCGATGT is restricted to a narrow domain centered around O4′-endo geometry.

The fact that the sugar puckers can be established fairly precisely by using at least three different J values (H1′–H2′, H2″–H3′, and H3′–H4′) from COSY and at least two r values (H1′–H4′ and H2″–H4′) from NOESY points to the power of 2D NMR techniques in obtaining the structure and dynamics of deoxyribose rings in DNA. It may be added that the five cross-peaks mentioned above fall in different spectral regions of the 2D spectra, which can be helpful in resolving

Table III

(A) Experimentally Observed and Theoretically Expected Intrasugar Interproton Distances (Å) in d-ACATCGATGT at 25 °C[a]

nucleotide unit	H1′–H2′	H1′–H2″	H1′–H3′	H1′–H4′	H2″–H4′
		Experimental Values			
A1	o	o	a	2.6 (2.9)	a
C2	2.9 (3.2)	2.4 (2.7)	a	o	a
A3	2.9 (3.2)	2.4 (2.7)	a	3.1 (3.4)	a
T4	2.8 (3.2)	2.4 (2.7)	a	2.7 (3.0)	a
C5	2.7 (3.0)	2.3 (2.6)	a	o	a
G6	3.0 (3.3)	2.5 (2.8)	a	2.7 (3.0)	a
A7	2.8 (3.0)	2.3 (2.6)	a	o	a
T8	2.8 (3.1)	2.4 (2.8)	a	2.7 (3.0)	a
G9	o	o	a	2.9 (3.2)	a
G10	o	o	a	2.6 (2.9)	a
		Theoretical Values			
C3′-endo	2.8	2.3	3.8	3.7	2.9
O4′-endo	3.0	2.3	4.0	2.8	3.5
C1′-exo	3.0	2.3	3.8	3.0	3.8
C2′-endo	3.0	2.3	3.8	3.4	4.2

(B) Intranucleotide Nonexchangeable Proton–Proton Distances (Å) in d-ACATCGATGT at 25 °C, Using C(H5–H6) and T(H6–CH3) (Values in Parentheses) Distances as Standard

nucleotide unit	H6/H8–H1′	H6/H8–H2′	H6/H8–H2″	H6/H8–H3′
A1	2.8 (3.2)	2.3 (2.6)	3.0 (3.4)	3.3 (3.7)
C2	w	2.2 (2.5)	w	a
A3	3.3 (3.8)	2.9 (3.3)	3.2 (3.6)	3.3 (3.7)
T4	3.2 (3.7)	2.4 (2.7)	3.3 (3.8)	a
C5	w	o	o	a
G6	2.9 (3.3)	2.3 (2.6)	o	3.2 (3.6)
A7	3.6 (4.1)	2.3 (2.6)	3.2 (3.6)	3.1 (3.5)
T8	3.6 (4.1)	2.5 (2.9)	3.2 (3.6)	a
G9	3.0 (3.3)	o	o	3.2 (3.5)
T10	3.2 (3.6)	o	o	a

(C) Internucleotide Nonexchangeable Proton–Proton Distances (Å) in d-ACATCGATGT at 25 °C, Using C(H5–H6) and T(H6–CH_3) (Values in Parentheses) Distances as Standard

base step	H6/H8–H1′	H6/H8–H2′	H6/H8–H2″	H6/H8–H8/H6/CH_3
C2–A1	a	3.0 (3.3)	3.0 (3.3)	a
A3–C2	w	3.6 (3.9)	3.3 (3.7)	a
T4–A3	3.1 (3.6)	3.0 (3.3)	2.7 (3.0)	2.7 (3.0)
C5–T4	a	o	o	a
G6–C5	a	3.8 (4.2)	2.9 (3.3)	a
A7–G6	2.8 (3.2)	o	2.7 (3.0)	a
T8–A7	3.4 (3.9)	3.6 (3.9)	2.7 (3.1)	2.9 (3.3)
G9–T8	a	o	3.2 (3.6)	a
T10–G9	3.2 (3.6)	o	o	3.1 (3.5)

[a] a = peak absent (proton–proton distance is greater than 4 Å), o = peaks overlap, w = weak peak. Experimental distances are estimated with cytosine H6–H5 and thymine H6–CH_3 (shown in parentheses) as reference scales.

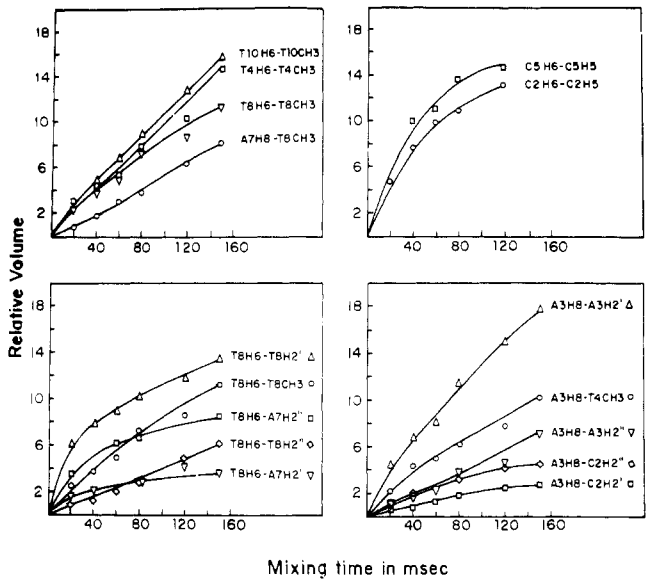

FIGURE 6: Buildup of normalized volumes of some intranucleotide and internucleotide NOESY cross-peaks in d-ACATCGATGT as a function of mixing time.

problems where there are spectral overlaps in one region or the other.

(f) Glycosidic Torsion Angle (χ). The intranucleotide distances between the base proton (H6 for pyrimidines and H8 for purines) and the sugar protons (H1′, H2′, H2″, H3′, and H4′) depend on the sugar pucker (P) as well as on the glycosidic torsion angle (χ). Such distances can be used, therefore, to fix angles χ once the sugar puckers have been established. The observed distances as measured from NOESY data can be interpreted with the help of simulated isodistance contours in the P,χ space.

The functional dependence of base to sugar distances has been simulated by using procedures already outlined. Figure 9 shows the behavior for the pyrimidine H6 proton. As expected, the isodistance contours for the purine H8 proton are similar. For any particular P,χ values, the H8 distance is usually larger than the corresponding H6 distance by about 0.2 Å. Therefore, only the pyrimidine curves have been discussed here. For accurate measurements, however, it is advisable to use the actual contours simulated for purines (supplementary material). While similar calculations have been reported by Wüthrich (1986), there are quantitative differences between his results and ours. One of the problems in such simulations where the pseudorotational concept is used for estimating individual torsional angles in the five-membered ring is that the ring closure may not be perfect. We have taken precautions to ensure the ring closure, and therefore we feel that the simulations presented here are more accurate.

We note that at low mixing times such as the one used here NOESY cross-peaks corresponding to $r > 4.0$ Å are expected to be absent. The thymine H6–CH_3 distance of 3.0 Å therefore is intermediate between the usual range of 2–4 Å where the NOESY cross-peaks have to be interpreted. The thymine cross-peaks can therefore serve as useful markers in qualitative descriptions of cross-peak intensities (i.e., weak or strong), although for accurate distance measurements, the cytosine scale may be better. Accordingly, we have classified regions in Figure 9 into three areas: $r > 4$ Å (no NOESY cross-peaks); $3 < r < 4$ Å (weak cross-peaks); and $r < 3$ Å (strong cross-peaks). Coupled with the knowledge of P values, such a qualitative description can be quite helpful in estimating χ values. For example, the H6–H1′ distance is within the observable NOESY limits over the entire range of χ values. This distance does not depend on sugar pucker and varies between 2.2 and 3.7 Å depending on χ. Strong cross-peaks are expected in the syn domain (χ = 0–120°), while weak peaks are expected in the anti domain (χ = 20° to −180°). The values of r(H6–H2′) are not very sensitive to the angle P, but only 50% of the area covered by the P,χ map can lead to significant NOESY cross-peaks. This area lies mostly in the anti domain of χ. The minimum value of r(H6–H2′) of 1.4 Å occurs around P = 220° and χ = −70°. However, strong NOESY peaks can arise from a much wider area roughly located between the axes χ = 0° and −140°. The remaining three distances r(H6–H2″), r(H6–H3′), and r(H6–H4′) show stronger dependence on P and χ. An ellipsoidal region centered around P = 145° and χ = −35° can lead to strong NOESY H6–H2″ peaks. The remaining area located roughly between χ = −140° and χ = −70° can lead to weak cross-peaks. Likewise, strong H6–H3′ cross-peaks are expected from a small region centered around P = 330° and χ = −110°. The distance increases quite rapidly as one moves in either direction from this point. Finally, the H6–H4′ distances are large in the entire P,χ hyperspace, though weak cross-peaks can be expected when P = 280° and χ = −150°.

In the present studies, we have observed that the individual sugar geometries are confined to a narrow region with P = 90–120°. One can then traverse the χ axis and compare the simulated experimental values to determine χ. In the following paragraphs we discuss this methodology.

Table IIIB shows that for the purine nucleotides (A1, A3, G6, A7, and G9) the H8–H1′ distances are in the range 2.8–3.6 Å (using the H5–H6 scale). The values of r(H8–H2′)

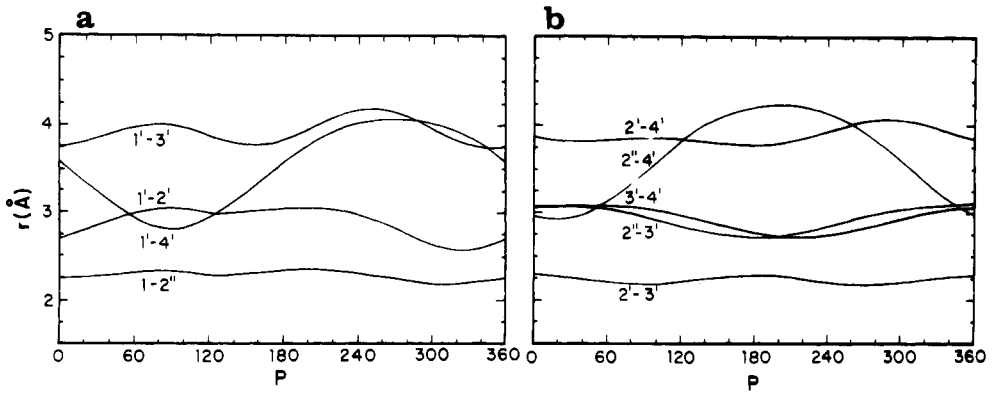

FIGURE 7: Calculated intrasugar ring interproton distances plotted as a function of pseudorotation phase angle (P): (a) 1′-2′, 1′–2″, 1′–3′, and 1′–4′ distances; (b) 2′–3′, 2″–3′, 2′–4′, 2′–4″, and 3′–4′ distances. These have been calculated by using a mononucleotide unit (dC) as a representative example, at regular intervals of 18° of P value. It is important in such simulations to check the closure of the sugar ring for each input datum, as was done in these calculations.

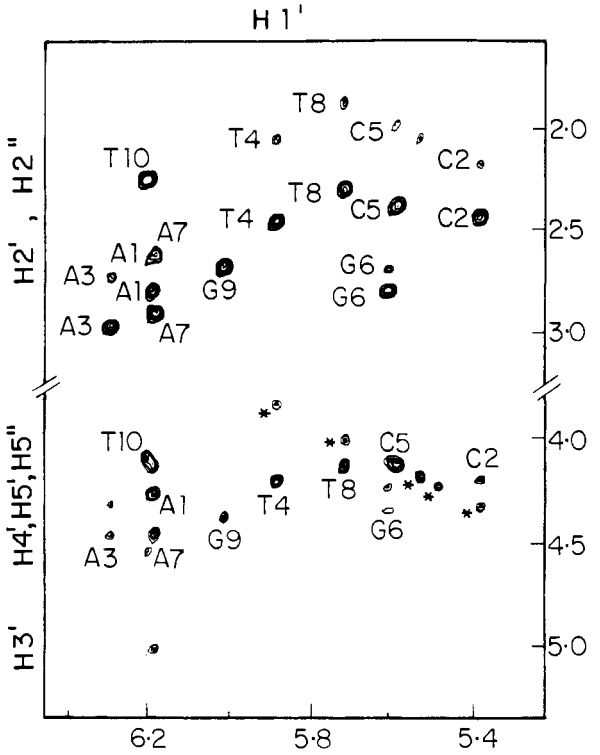

FIGURE 8: Expansion of selected regions of 500-MHz pure absorption mode ω_1-scaled NOESY spectrum of d-ACATCGATGT in ^2H_2O at 25 °C recorded with a mixing time of 80 ms. This panel contains all the expected NOESY cross-peaks from the H1′ proton to H2′, H2″, and H4′ protons. The starred peaks are artifacts arising from imperfections in quadrature detection.

in the case of A1, A3, G6, and A7 are in the range 2.3–2.9 Å, while the values of r(H8–H2″) for these four nucleotides lie in the range 3.0–3.2 Å. For G9, the near equivalence of H2′ and H2″ makes it impossible to estimate the H8–H2′ and H8–H2″ distances. The H8–H3′ distances lie in the range 3.1–3.3 Å. We do not observe H8–H4′ cross-peaks. These results are consistent with χ values of $-120° \pm 20°$.

The situation for pyrimidines is more complicated primarily because of peak overlaps and weak intensities of NOESY cross-peaks. At low mixing times, both the H6–H3′ and the H6–H4′ cross-peaks are absent. The H6–H1′ distance has been measured for T4 (r = 3.2 Å), T8 (r = 3.6 Å), and T10 (r = 3.2 Å). In the case of C2 and C5, the H6–H1′ cross-peaks are very weak. The H6–H2′ distances have been measured for C2 (r = 2.2 Å), T4 (r = 2.4 Å), and T8 (r = 2.5 Å). In the case of C5 and T10, peak overlaps make it difficult to measure such distances. Likewise, H6–H2″ distances have been measured only for T4 (r = 3.3 Å) and T8 (r = 3.2 Å). The cross-peak corresponding to C2 is weak, while the problem of insufficient resolution is encountered in the case of the other two pyrimidines. The observed distances are consistent with χ in the anti domain with values close to those observed for purines, although the precision is lower for pyrimidines.

(*g*) *Backbone Torsion Angle.* We propose a homonuclear 2D J,δ spectrum to monitor the ^{31}P–^1H heteronuclear couplings that are preserved in the ω_2 projection (R. V. Hosur, K. V. R. Chary, A. Saran, G. Govil, and H. T. Miles, unpublished results). This projection helps in resolving the ^{31}P–H3′ coupling constants to a large extent (Figure 10). With the knowledge of the sequential resonance assignments described earlier, these coupling constants could be identified for individual pairs of ^{31}P–H3′. Thus, the ^{31}P–H3′ coupling constants have been measured and found to be around 4 Hz in the case

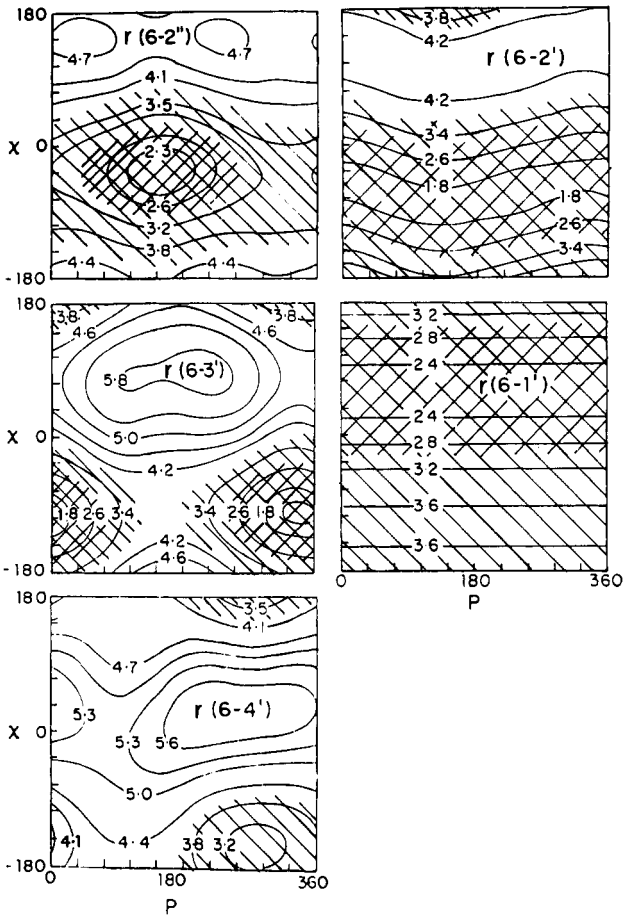

FIGURE 9: Theoretically calculated two-dimensional distance contours depicting the dependence of intranucleotide proton–proton distances between the base (H6) and the sugar (H1′, H2′, H2″, H3′, and H4′) protons on the pseudorotation phase angle (P) and glycosidic bond torsional angle (χ) for pyrimidines. The maps shown here refer to pyrimidines (C and T). The H8–sugar distances in purines are usually 0.2 Å larger than the corresponding H6–sugar distances in pyrimidines. The areas are shaded to reflect different levels of expected cross-peak intensity.

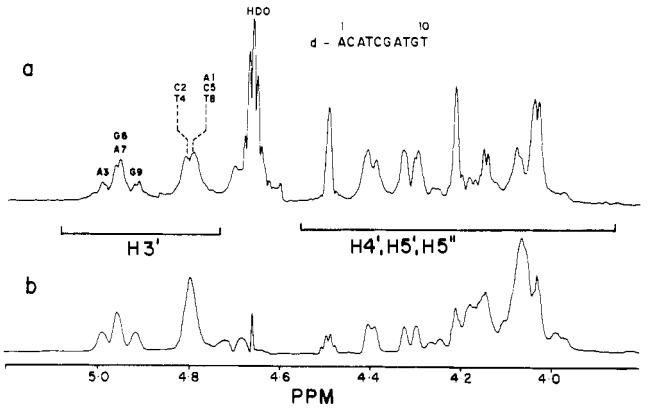

FIGURE 10: Comparison of ω_2 projection of homonuclear (J, δ) spectrum (a) of d-ACATCGATGT with the corresponding one-dimensional ^1H spectrum (b), both recorded in ^2H_2O solution at 35 °C. Sequence-specific assignments are indicated for the H3′ protons. The H3′ chemical shifts of G6 and A7, C2 and T4, and A1, C5, and T8 are identical.

of all nucleotide units except T10. This information has been used to quantify the C4′–C3′–O3′–P backbone torsion angle (ϵ) by using the Karplus-type relation

$$J = 16.3 \cos^2 \theta - 4.6 \cos \theta$$

where θ is the torsion angle in the related atom sequence

Table IV

(A) Comparison of Intranucleotide Distances (Å) between Nonexchangeable Protons in d-ACATCGATGT with Different DNA Models and d-GGTACGCGTACC

distance	A-DNA, $p = 18°$, $\chi = -156°$	B-DNA, $p = 162°$, $\chi = -117°$	DNA, $p = 90°$, $\chi = -135°$	d-GGTACGCGTACC	d-ACATCGATGT
H6–H1′	3.5	3.7	3.7	3.6–3.7	3.6–3.8
H8–H1′	3.7	3.7	3.7	3.6–3.9	3.6–3.8
H6–H2′	3.8	2.0	2.5	2.6–2.8	2.4–2.8
H8–H2′	3.8	2.2	2.6	2.6	2.6–2.8
H6–H2″	4.4	3.4	3.9	3.6–3.9	3.4–3.8
H8–H2″	4.5	3.6	4.1	3.7	3.8

(B) Comparison of Internucleotide Distances (Å) between Nonexchangeable Protons in d-ACATCGATGT with Those of Standard A-DNA, B-DNA, and d-GGTACGCGTACC

distance	A-DNA[a]	B-DNA[a]	d-GGTACGCGTACC	d-ACATCGATGT
H6–H1′	2.6	3.5	3.4–4.0	3.6–3.9
H8–H1′	4.6	3.6	3.4–3.8	3.2
H6–H2′	2.0	4.0	3.3–3.6	3.3
H8–H2′	2.1	3.8	3.4–3.6	3.9–4.2
H6–H2″	3.7	2.2	2.9–3.6	3.0–3.4
H8–H2″	3.9	2.1	3.2–3.4	3.0–3.6
CH_3–H8	3.4	3.8	3.2–3.5	2.9–3.5

[a] Wüthrich (1986).

H3′–C3′–O3′–P (Hosur et al., unpublished results). According to this equation, a value of 4 Hz for the H3′-^{31}P coupling constant corresponds to ϵ torsion angle in the ranges 150–200° or 300–350°. Although the H3′–^{31}P coupling constant alone cannot distinguish between the two domains, we feel that ϵ is in the range 150–200° because of the high frequency of crystal structure data around this value in several oligonucleotides studied under different conditions.

Because of the strong coupling effects between H5′ and H5″ resonances, it has been impossible to resolve the ^{31}P–H5′, H5″ couplings, and hence the corresponding torsion angle could not be measured.

(*h*) *Comparison of the Conformation of d-ACATCGATGT with Different DNA Models and d-GGTACGCGTACC.* It may be recalled that once the sugar conformation, glycosidic dihedral angles, and ϵ are fixed, one is left with only four backbone torsion angles to complete the 3D structures of individual nucleotides. In favorable cases four sequential internucleotide distances (base–H1′, base–H2′, base–H2″, and base–base) can be obtained. In such situations, the experimental data are sufficient in principle to fix the backbone geometry uniquely. Nevertheless, because of uncertainties in distance estimates and peak overlaps it has not yet been possible to accomplish this in practice. We therefore adopt here the approach of comparing our results with known DNA structures.

In Table IVA we compare the intranucleotide proton–proton distances for different DNA models and d-GGTACGCGTACC with the observed distances for the present decamer. Though the base (H6/H8)–H1′ and H2″ distances are similar to those for a standard B-DNA structure, the base (H6/H8)–H2′ distances are strikingly different. In our studies on d-GGTACGCGTACC (Chary et al., 1988) we attributed the discrepancy in the values of (H8/H6)–H2′ distance to the differences in the sugar pucker present in the dodecamer (i.e., close to O4′-endo) and that used in the B-DNA model (close to C2′-endo). It is evident from Table IVA that all the observed intranucleotide proton–proton distances in the present decamer are similar to those in d-GGTACGCGTACC. To quantify such sugar-pucker dependence of intranucleotide proton–proton distances, we have compared these experimental distances with theoretically calculated values with $P = 90°$ and $\chi = -135°$ (which are the experimentally found P and χ values). For such a pair of P and χ values the observed distances correspond to the theoretical values.

Table IVB shows the comparison of internucleotide distances between nonexchangeable protons in d-ACATCGATGT with those of different DNA models and d-GGTACGCGTACC. As in the case of intranucleotide distances, the internucleotide distances also show a reasonable correspondence with the estimated distances for a standard B-DNA model except $(H8/H6)_{i+1}$–$(H2')_i$ distances. This we attribute to the combined effect of different backbone torsion angles including the sugar puckers.

Conclusions

We have tried to obtain the maximum possible information on the solution conformation of d-ACATCGATGT entirely from 2D NMR. At the level described in this paper, we are able to fix the pseudorotation phase angles (P) and the glycosidic bond torsion angles (χ), and some limits have been obtained for one of the backbone torsion angles (ϵ). We can also obtain four sequential internucleotide (intrastrand) distances. From the observation of imino proton resonances in 80% H_2O plus 20% ^2H_2O, the existence of hydrogen-bonded base pairs is confirmed. The observed internucleotide distances provide information about the directionality of the helix. For example, the interbase distances, namely, A3H8 → T4CH_3, A7H8 → T8CH_3, and G9H8 → T10CH_3, indicate that the molecule is a right-handed helix. Further, it is evident from the variations in the distances that there are small but finite differences in the backbone torsion angles along the sequence of the molecule. The present strategies thus provide an approach toward complete solution of the DNA structure entirely from the NMR data.

Acknowledgments

The facilities provided by the 500-MHz FTNMR National Facility supported by the Department of Science and Technology, Government of India, are gratefully acknowledged.

Supplementary Material Available

Theoretically calculated 2D space contours depicting the dependence of intranucleotide proton–proton distances (1

page). Ordering information is given on any current masthead page.

Registry No. α-ACATCGATGT, 116169-79-0.

REFERENCES

Altona, C., & Sundaralingam, M. (1972) *J. Am. Chem. Soc. 94*, 8205–8212.

Atkinson, T., & Smith, M. (1984) in *Oligonucleotide Synthesis. A Practical Approach* (Gait, M. J., Ed.) IRL, Oxford, U.K.

Bax, A., & Freeman, R. (1981) *J. Magn. Reson. 44*, 542–561.

Chary, K. V. R., & Modi, S. (1988) *FEBS Lett. 233*, 319–325.

Chary, K. V. R., Hosur, R. V., Govil, G., Tan, Z-k., & Miles, H. T. (1987) *Biochemistry 26*, 1315–1322.

Chary, K. V. R., Hosur, R. V., Govil, G., Chen, C., & Miles, H. T. (1988) *Biochemistry 27*, 3858–3867.

Chazin, W. J., Wüthrich, K., Hybert, S., Rance, M., Denny, W. A., & Leupin, W. (1986) *J. Mol. Biol. 19*, 439–453.

Clore, G. M., Gronenborn, A. M., & Mclaughlin, L. W. (1985a) *Eur. J. Biochem. 151*, 153–165.

Clore, G. M., Gronenborn, A. M., Moss, D. S., & Tickle, I. J. (1985b) *J. Mol. Biol. 185*, 219–226.

Feigon, J., Wright, J. M., Leupin, W., Denny, W. A., & Kearns, D. R. (1982) *J. Am. Chem. Soc. 104*, 5540–5541.

Feigon, J., Denny, W. A., Leupin, W., & Kearns, D. R. (1983a) *Biochemistry 22*, 5930–5942.

Feigon, J., Leupin, W., Denny, W. A., & Kearns, D. R. (1983b) *Biochemistry 22*, 5943–5951.

Frechet, D., Cheng, D. M., Kan, L. S., & Ts'o, P. O. P. (1983) *Biochemistry 22*, 5194–5200.

Govil, G., & Hosur, R. V. (1982) *Conformation of Biological Molecules*, Springer, Heidelberg.

Hare, D. R., Wemmer, D. E., Chou, S. H., Drobny, G., & Reid, B. R. (1983) *J. Mol. Biol. 171*, 319–336.

Hare, D. R., Shapiro, L., & Patel, D. J. (1986a) *Biochemistry 25*, 7445–7456.

Hare, D. R., Shapiro, L., & Patel, D. J. (1986b) *Biochemistry 25*, 7456–7474.

Hore, P. J. (1983) *J. Magn. Reson. 55*, 283–300.

Hosur, R. V., Ravikumar, M., Roy, K. B., Tan, Z-k., Miles, H. T., & Govil, G. (1985a) in *Magnetic Resonances in Biology and Medicine* (Govil, G., Khetrapal, C. L., & Saran, A., Eds.) pp 243–260, Tata McGraw-Hill, New Delhi.

Hosur, R. V., Chary, K. V. R., Kumar, A., & Govil, G. (1985b) *J. Magn. Reson. 62*, 123–127.

Hosur, R. V., Chary, K. V. R., & Ravikumar, M. (1985c) *Chem. Phys. Lett. 116*, 105–108.

Hosur, R. V., Ravikumar, M., Chary, K. V. R., Sheth, A., Govil, G., Tan, Z-k., & Miles, H. T. (1986a) *FEBS Lett. 205*, 71–76.

Hosur, R. V., Sheth, A., Chary, K. V. R., Ravikumar, M., Govil, G., Tan, Z-k., & Miles, H. T. (1986b) *Biochem. Biophys. Res. Commun. 139*, 1224–1232.

Hosur, R. V., Chary, K. V. R., Majumdar, A., & Govil, G. (1988a) *Life Sci. Adv.* (in press).

Hosur, R. V., Chary, K. V. R., Sheth, A., Govil, G., & Miles, H. T. (1988b) *J. Biosci. 13*, 71–86.

Kumar, A., Wagner, G., Ernst, R. R., & Wüthrich, K. (1981) *J. Am. Chem. Soc. 103*, 3654–3658.

Kumar, A., Hosur, R. V., & Chandrasekhar, K. (1984) *J. Magn. Reson. 60*, 143–148.

Marion, D., & Wüthrich, K. (1983) *Biochem. Biophys. Res. Commun. 113*, 967–974.

McBride, L. J., & Caruthers, M. H. (1983) *Tetrahedron Lett. 24*, 245–248.

Ravikumar, M., Hosur, R. V., Roy, K. B., Miles, H. T., & Govil, G. (1985) *Biochemistry 24*, 7703–7711.

Redfield, A. G., & Kunz, S. D. (1975) *J. Magn. Reson. 19*, 250–254.

Reid, D. G., Salisbury, S. A., Bellard, S., Shakked, Z., & Williams, D. H. (1983) *Biochemistry 22*, 2019–2025.

Rinkel, L. J., & Altona, C. (1987) *J. Biomol. Struct. Dyn. 4*, 621–649.

Saran, A., Perahia, D., & Pullman, B. (1973) *Theor. Chim. Acta 30*, 31.

Scheek, R. M., Russo, N., Boelens, R., Kaptein, R., & Van Boom, J. H. (1983) *J. Am. Chem. Soc. 105*, 2914–2916.

Scheek, R. M., Boelens, R., Russo, N., Van Boom, J. H., & Kaptein, R. (1984) *Biochemistry 23*, 1371–1376.

Sheth, A., Ravikumar, M., Hosur, R. V., Govil, G., Tan, Z-k., & Miles, H. T. (1987a) *Biochem. Biophys. Res. Commun. 144*, 26–34.

Sheth, A., Ravikumar, M., Hosur, R. V., Govil, G., Tan, Z-k., Roy, K. B., & Miles, H. T. (1987b) *Biopolymers 26*, 1301–1313.

Sinha, N. D., Biernat, J., McManus, J., & Kaster, H. (1984) *Nucleic Acids Res. 12*, 4539–4557.

Staehelin, M., Sober, H. A., & Peterson, E. A. (1959) *Arch. Biochem. Biophys. 85*, 289–291.

Tomlinson, R. V., & Tener, G. M. (1963) *Biochemistry 2*, 697.

Wagner, G., & Wüthrich, K. (1979) *J. Magn. Reson. 33*, 675–680.

Wüthrich, K. (1986) *NMR of Proteins and Nucleic Acids*, pp 203–220, Wiley-Interscience, New York.

Wynants, C., & Van Binst, G. (1984) *Biopolymers 23*, 1979–1804.